Journal of Materials Chemistry C

ROYAL SOCIETY OF CHEMISTRY

PAPER

View Article Online
View Journal

Cite this: DOI: 10.1039/d5tc04271b

Unveiling the multifunctional properties of dicyanoisophorone derivatives: from white OLEDs and picric acid sensing to nonlinear optics

Khushdeep Kaur, [a] Oleksandr Bezvikonnyi, [ab] Dmytro Volyniuk, [a] Weizhen Liu, [c] Yovan de Coene, [c] Koen Clays, *[c] Kamaljit Singh, [d] Ehsan Ullah Rashid, [a] Asta Dabuliene, [a] Oleksandr Navozenko [e] and Juozas V. Grazulevicius *[a]

Received 4th December 2025,
Accepted 5th February 2026

DOI: 10.1039/d5tc04271b

rsc.li/materials-c

Newly designed and synthesized derivatives of dicyanoisophorone and different donors, *i.e.*, phenylcarbazole, fluorene, phenanthrene and dimethylfluorene, are characterized by high thermal stability and exhibit aggregation-induced emission enhancement. White organic light-emitting diodes with the derivative of fluorene and dicyanoisophorone as the emitter, operating *via* hybridized local and charge transfer states, are characterized by a color rendering index of 82. The emitter is also used for the detection of picric acid with Stern–Volmer constants of 16.2×10^4 and 2.7×10^3 M^{-1}. The structure-dependent nonlinear optical response with β_{zzz} values in the range of 785–1901 $\times$ 10^{-30} esu measured using the hyper-Rayleigh scattering (HRS) technique reflects the multifunctional potential of these materials.

1. Introduction

The technology of organic light-emitting diodes (OLEDs) has gained an established position in the market for displays. The application of white OLEDs (WOLEDs) for lighting is challenging, mostly due to issues related to cost-effectiveness.[1] White emission is conventionally achieved in WOLEDs by incorporating a multilayer structure with different emitters, commonly RGB.[2,3] Occasionally, it requires the utilization of exciplexes.[4,5] All of these factors complicate the device structure. A color rendering index (CRI) of 80 is required for typical luminaries.[6] The development of relatively simple emitting systems for white electroluminescent (EL) devices with satisfactory characteristics of efficiency and color quality has become an important topic of research.[7]

A great deal of attention has been paid to organic materials that are non-emissive or low-emissive when dissolved in solvents but exhibit a high quantum yield in the solid state. In recent decades, solid-state luminescence enhancement (SSLE) has been widely studied and utilized in various optical devices.[8,9] The more common term for the phenomenon is aggregation-induced emission enhancement (AIEE). The primary reason for this phenomenon is generally considered to be the restriction of vibrational and rotational motions in the aggregated (solid) state.[10] AIEE is the converse of aggregation-caused quenching, a property commonly observed for organic emitters.[11] Due to their useful properties, emitters exhibiting AIEE were developed for application in WOLEDs.[10]

The development of nonlinear optically (NLO)-active organic chromophores is a significant objective owing to their diverse applications in telecommunication, data storage, next-generation integrated photonic circuits, signal processing, and terahertz (THz) generation.[12,13] Second-harmonic generation (SHG) is the most diversely studied second-order NLO effect in which frequency up-conversion is observed when an intense incident laser pulse interacts with such materials.[14] On the molecular level, it requires a nonzero hyperpolarizability β, whereas the supramolecular organization should exhibit a non-zero second-order NLO susceptibility, χ^2.[15] A critical choice of donor (D) and acceptor (A) components remains a challenge in the pursuit of designing efficient NLO-active materials. Such compounds must comprise a large first hyperpolarizability, β, as it demands a well-balanced trade-off between the conjugation path length, D–A strengths, and asymmetric electronic distribution.[16]

[a] Department of Polymer Chemistry and Technology, Faculty of Chemical Technology, Kaunas University of Technology, K. Baršausko st. 59, LT-51423 Kaunas, Lithuania. E-mail: juozas.grazulevicius@ktu.lt
[b] Institute of Solid State Physics, University of Latvia, Kengaraga 8, LV-1063, Riga, Latvia
[c] Department of Chemistry, University of Leuven, Celestijnenlaan 200D, B-3001 Leuven, Belgium. E-mail: Koen.Clays@kuleuven.be
[d] Department of Chemistry, UGC Centre of Advanced Study, Guru Nanak Dev University, Amritsar 143005, India
[e] Department of Experimental Physics, Faculty of Physics, Taras Shevchenko National University of Kyiv, Akademika Glushkova Av. 4, 03127, Kyiv, Ukraine

Dicyanoisophorone is a well-known electron acceptor used as a structural unit of compounds intended for sensing, bioimaging, *etc.*[17] Dicyanoisophorone-based luminophores mostly adopt a donor–π–acceptor (D–π–A) structure. They are characterized by intramolecular charge transfer (CT) emission and a large Stokes shift.[17] The dicyanoisophorone moiety has also been used as an acceptor fragment for the development of AIEEgens[18,19] and efficient NLOphores.[16,20]

Herein, we report a series of dicyanoisophorones with different donor moieties attached as emitters exhibiting AIEE. In particular, the electron-donating units of phenylcarbazole, fluorene, phenanthrene, and dimethylfluorene were used in the design of compounds as the (hetero)aromatic moieties. They are widely used as the moieties inducing AIEE.[10,21–23] One of the compounds was used in a detection system of picric acid and as an emitter in WOLED. However, the potential of these D–A fragments as NLO-active chromophores remains relatively underexplored.

Developing systems for the detection of nitroaromatic explosive materials is a research topic of great interest.[24,25] Its importance arises from security objectives to determine traces of explosive materials in protected areas, track down the location of land mines, and so on. Organic emitters exhibiting AIEE were reported as sensitivity probes for the detection of picric acid.[11,21,26–29] To the best of our knowledge, dicyanoisophorone derivatives have not been used yet either for the detection of picric acid or for the fabrication of WOLEDs.

In optoelectronic devices, the ratio of singlet and triplet excitons generated is statistically 1 : 3.[30] Triplet excitons do not conventionally take part in emissive processes, forcing the studies to aim at the stimulation of triplet-facilitated emission.[6,30–36] Emitters exhibiting hybridized local and charge transfer (HLCT) states or the so-called hot excitons are widely developed, as this phenomenon allows to upconvert triplet excitons to the singlet excited states *via* reverse intersystem crossing at high energy levels.[6,30,36,37] The dicyanoisophorone derivatives as HLCT-exhibiting luminophores were not reported before. The precise molecular engineering involving the abovementioned donor units along with a dicyanoisophorone acceptor remains elusive, to the best of our knowledge.

2. Experimental

A detailed description of the instruments is given in the SI (Section S1).

3. Results and discussion

3.1. Synthesis, thermal, electrochemical, and CT properties

Derivatives of dicyanoisophorone and of the different donors, namely, phenylcarbazole (K1), fluorene (K2), phenanthrene (K5), and dimethylfluorene (K6), were designed and synthesized as emitters exhibiting SSEE. The compounds were synthesized based on (*E*)-2-(3-(4-bromostyryl)-5,5-dimethylcyclohex-2-en-1-ylidene)malononitrile (Br-Ph-ISP) using the Suzuki cross-coupling reaction. The details of synthesis of the derivatives of dicyanoisophorone K1, K2, K5 and K6 are given in Scheme 1 and the SI (Section S2).

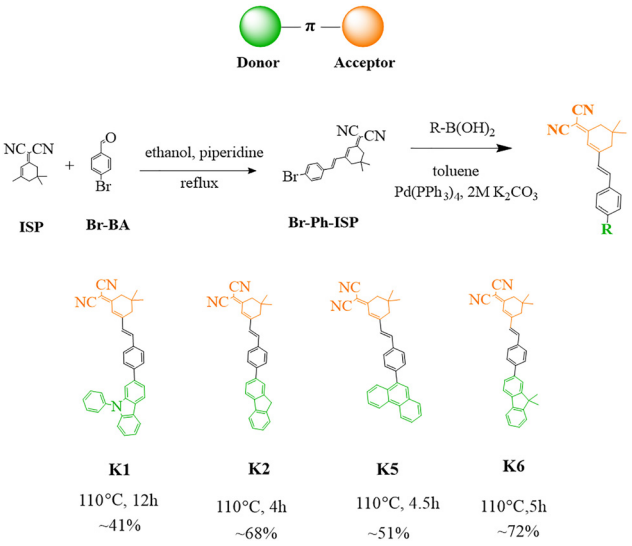

Scheme 1 Synthesis of K1–K6.

The thermal characteristics of the synthesized compounds were estimated by thermogravimetric analysis (TGA) and differential scanning calorimetry (DSC) (Fig. 1 and Fig. S20). They are summarized in Table 1. All the compounds exhibited relatively high thermal stability. The 5% weight-loss temperatures (T_{ID}) were found to be in the range of 345–378 °C. Compounds K1, K2, and K5 exhibited close values of T_{ID}, whereas K6 showed slightly lower thermal stability. In the first heating scans of DSC (Fig. 1 and Fig. S20b) moderately high melting temperatures (T_{mp}) of 225–298 °C were observed for K1, K2, and K6, whereas K5 displayed a lower T_{mp} of 203 °C. Upon cooling, K2 and K6 exhibited crystallization signals (T_{cr}) at 252 and 185 °C, respectively. Meanwhile, the samples of K1 and K5 did not give any signals of crystallization, implying the formation of molecular glasses. Except for K2, glass transitions were observed for K1, K5, and K6 at 113, 98, and 99 °C, respectively. The lower T_{mp}, T_{cr}, and T_{ID} values of K6 relative to those of K2 and the capability of glass formation of the former compound clearly reveal the effect of methylation of the fluorene donor moiety of K6. This observation can be attributed to a disruption in the

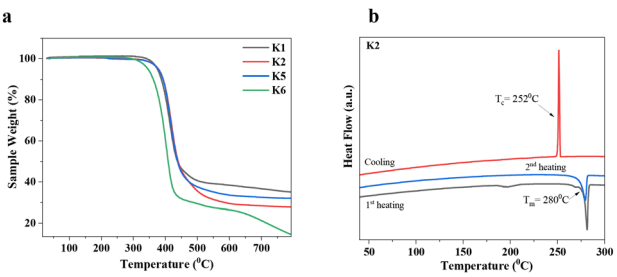

Fig. 1 (a) TGA curves recorded at the heating rate of 20 °C min^{-1} in a nitrogen atmosphere for K1, K2, K5 and K6 (a). (b) DSC thermograms of K2 recorded at a heating rate of 10 °C min^{-1} in a nitrogen atmosphere.

Table 1 Characteristics of K1, K2, K5, and K6

Compound	T_{ID}, °C	T_{mp}, °C	T_{cr}, °C	T_g, °C	E_{ox}^{onset}, V	IE_{CV}, eV	E_{red}^{onset}, eV	EA_{CV}, eV	$HOMO_{DFT}$, eV	$LUMO_{DFT}$, eV	Φ_{tol}	Φ_{film}	Φ_{Zeonex}
K1	374	298	—	113	1.30	5.78	−0.90	3.58	−5.44	−2.79	*ca.* 0	0.05	0.06
K2	377	280	252	—	1.43	5.91	−0.88	3.60	−5.78	−2.86	*ca.* 0	0.07	0.05
K5	378	203	—	98	1.56	6.04	−0.87	3.61	−5.76	−2.89	*ca.* 0	0.02	0.02
K6	345	227	185	99	1.48	5.96	−0.84	3.64	−5.77	−2.86	*ca.* 0	0.04	0.04

T_{cr} of 252 °C for K2 is observed during the cooling scan. T_{cr} of 185 °C for K6 is observed during the second heating scan. T_g values are observed during the second heating scan. $IE_{CV} = E_{ox}^{onset} - E_{ox}$ (ferrocene) + 4.8. $EA_{CV} = E_{red}^{onset} - E_{ox}$ (ferrocene) + 4.8.

rigid molecular packing in K6 upon the introduction of methyl groups.

Cyclic voltammetry measurements of 10^{-3} M DCM solutions of the studied compounds were carried out by applying positive and negative voltages to estimate their redox behavior (Fig. 2a). Their respective ionization potential IP_{CV} and electron affinity EA_{CV} values were calculated (Table 1). All the compounds showed irreversible oxidation and reduction peaks corresponding to the respective electron transfer processes. Oxidation onset potentials for K1, K2, K5, and K6 were found to be 1.30, 1.43, 1.56, and 1.48 V, respectively. Considering the oxidation onset potentials of the internal reference (Fc/Fc^+), IE_{CV} values were calculated to be 5.78, 5.91, 6.04, and 5.96 eV for K1, K2, K5, and K6, respectively. The EA_{CV} values were calculated to be 3.58, 3.60, 3.61, and 3.64 eV, corresponding to reduction onset potentials of −0.90, −0.88, −0.87, and −0.84 V for K1, K2, K5, and K6, respectively. These values were found to be close owing to the presence of the same electron-accepting unit.

The ionization energies of the synthesized compounds ranged from 5.78 eV to 6.04 eV. K1 exhibited the lowest ionization energy. This observation can be explained by the enhanced electron density of the N-substituted carbazole unit taking part in delocalization as well as the electron transfer process. Fluorene, phenanthrene, and 9,9-dimethylfluorene donor units of the compounds K2, K5, and K6 have no heteroatoms, making them less electron-rich and, hence, difficult to oxidize. The experimental data are consistent with the values theoretically calculated using density functional theory (DFT) at the B3LYP/6-31G(d,p) level of theory (Table 1 and Fig. 3).

According to the results of the time-of-flight (TOF) and charge carrier extraction by linearly increasing voltage (CELIV) experiments, the layer K2 exhibited the highest values of hole and electron mobilities (Fig. 2b and Fig. S21). Additionally, well-balanced hole and electron mobilities of 3×10^{-5} and 5.3×10^{-5} $cm^2 V^{-1} s^{-1}$, respectively, at an electric field of 5.85×10^5 $V cm^{-1}$ were observed for K2, making it the most promising candidate for OLED applications. The results of the TOF and CELIV measurements performed for K1, K2, K5, and K6 are discussed in more detail in the SI (Section S4).

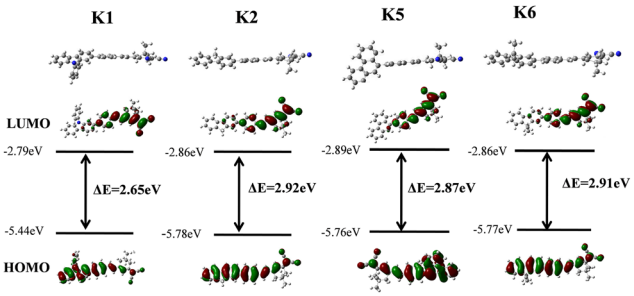

Fig. 3 Global minimized structures and contour plots of the HOMO and LUMO of K1, K2, K5 and K6.

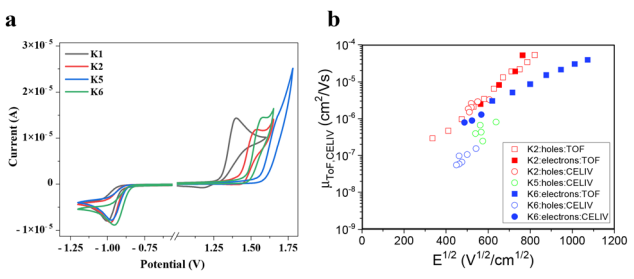

Fig. 2 (a) Cyclic voltammetry curves of dilute DCM solutions (10^{-3} M) of compounds K1, K2, K5 and K6. (b) Plots of hole and electron drift mobilities of the vacuum-deposited layers of K1, K2, K5 and K6 recorded by TOF or CELIV methods *versus* the electric field.

3.2. Linear optics, excited states, and AIEE

The absorption spectra of the films and dilute solutions of the compounds have signature peaks of the corresponding donor moieties (Fig. 4a). Hence, the absorption spectrum of the film of K1 contains bands at ∼265 and 320 nm associated with the $1L_a \leftarrow 1A$ and $1L_b \leftarrow 1A$ transitions of the phenylcarbazole fragment, respectively. They are blue shifted compared with the absorption bands of phenylcarbazole.[38] The absorption spectra of the dilute solutions of K2 have a characteristic double peak of the fluorene fragment at ∼300 nm.[39] The absorption band of the film of K2 is blue shifted with respect to those of the solutions. The set of the vibronic bands observed in the absorption spectra of the film and solutions of K5 in the range of 250–300 nm correspond to the electronic transition $2^1A_1(S_1) \leftarrow X^1A_1(S_0)$ of phenanthrene.[40] The absorption bands of the solutions of K6 peaking at ∼300 nm are associated with the π–π* transitions of dimethylfluorene.[38] The lowest energy bands of the absorption spectra of the films and solutions of the compounds are caused by the dicyanoisophorone moiety. For the films, they are redshifted relative to those of the corresponding dilute solutions. These bathochromic shifts and the presence of low-energy tails are explained by enhanced intermolecular interactions in the solid state. There is no clear correlation between the wavelengths of the lowest-energy

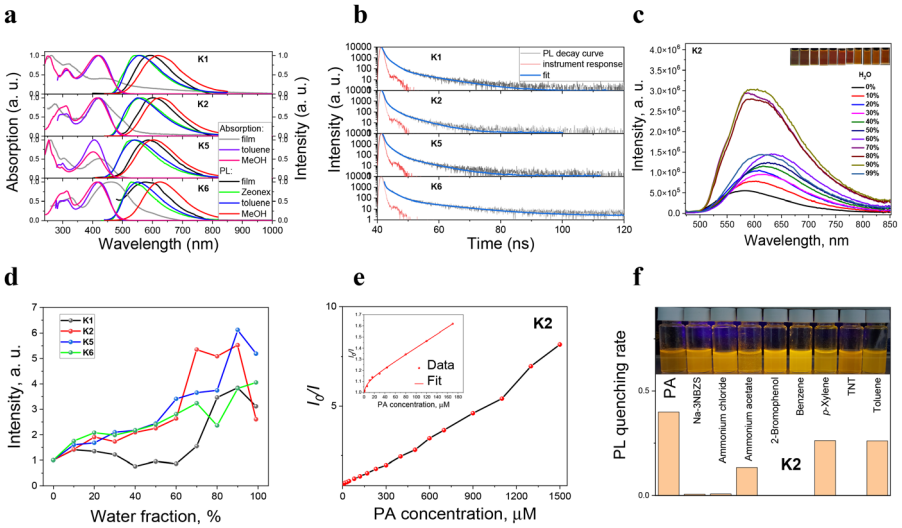

Fig. 4 (a) Absorption and PL spectra of the toluene 10^{-5} M solutions, neat films of the compounds and films of the compound doped in Zeonex (1 wt%). (b) PL decay curves of the neat films of the compounds recorded in air at room temperature. (c) PL spectra of the dispersions of K2 in the mixtures of THF and water for different water fractions (inset: photographs of the corresponding cuvettes), and (d) the corresponding plots of PL intensity *vs.* water volume fraction. (e) The Stern–Volmer plot of the PL spectra of the dispersions of K2 (10^{-4} M) and picric acid (PA) in the mixtures of THF (volume fraction, 5%) and water (volume fraction, 95%). (f) Competitive selectivity of the dispersions of K2 (1 mg mL^{-1}) in mixtures (2 mL) of THF (volume fraction, 5%), water (volume fraction, 94%), and acetonitrile (volume fraction, 1%) toward PA and various contaminants (20 μg) (inset: photographs of the corresponding bottles).

absorption peaks and solvent polarities (Fig. 4a). This points to the limited probability of the CT character of the band.

The PL spectra of the solutions of the compounds undergo significant redshifts in the peak positions upon increasing the polarity of the solvents. The shifts of up to 75 nm from the yellowish green to red spectral regions are observed (Fig. S22). This is a manifestation of the emission of the intramolecular CT states.[41] Toluene solutions of the compounds exhibit a slight increase in PL intensity after degassing due to a partial deactivation of the excited states by collisional interactions with molecular oxygen (Fig. S23).[42] The extent of emission enhancement indicates the limited involvement of the triplet states.[42] This indicates the utilization of HLCT states.

Fig. 4a shows the PL spectra of the films of the compounds (1 wt%) doped in Zeonex. Zeonex is a rigid polymer of low polarity that cuts off intermolecular interactions. Expectedly, the PL spectra of the films of the compounds doped in Zeonex are close to the emission spectra of dilute toluene solutions, as toluene has a negligible polarity, similar to Zeonex.[43] On the other hand, the PL spectra of the neat films of the compounds are bathochromically shifted from the spectra of the corresponding toluene solutions and the films of the compounds doped in Zeonex. This observation points to the effects of molecular packing in agreement with the CT nature of the emissions. The PL decay curves of the films of the compounds as well as films of the compound doped in Zeonex exhibited prompt fluorescence (Table S1 and Fig. 4b). The average lifetimes of the PL of the films slightly increased after evacuation (Table S1).

This observation indicates the utilization of triplet energy due to HLCT, as observed in the case of degassed toluene solutions (Fig. S23a–d). The signature of the manifestation of the HLCT states could be also experimentally observed in the Lippert–Mataga plots (Fig. S23e).[44–47]

The presence of HLCT states was further substantiated by theoretical calculations. DFT analysis (B3LYP/6-31G(d,p) indicated that the highest occupied molecular orbital (HOMO) is partially localized on the phenyl bridge and dicyanoisophorone alongside the donor moieties in all the compounds (Fig. 3). The lowest unoccupied molecular orbital (LUMO) is primarily located solely on the phenyl bridge and dicyanoisophorone moiety. This spatial distribution of the HOMO and LUMO is a preliminary indication of the mixture of the states of CT from the electron donor to accepting moieties, and the local excitation on the acceptor unit and phenyl bridge. Furthermore, natural transition orbitals (NTOs) of the main transition configuration (Fig. S27–S30) were analysed to elucidate the underlying nature of these electronic transitions. The primary ''hole'' and ''electron'' contributions of NTOs of the first excited states (ESs) of all molecules demonstrate that S_1 comprises a mixture of local excitation (LE) from the phenyl ring and CT from the respective donor units to the common dicyanoisophorone acceptor unit. Notably, the theoretically simulated UV spectra of K1–K6 (for toluene, see Fig. S27–S30) revealed that in addition to the lowest singlet excited states S_1 with oscillator strengths ($f_{S0\rightarrow S1}$) ranging from 0.5749 to 1.5235, higher electronic states of significant oscillator strengths (f = 0.0355 to 0.9719) also contribute appreciably toward their respective absorption profiles. These contributions from additional electronic states of higher energy to the UV spectra manifesting as enhanced spatial overlaps between the NTOs is a typical characteristic of HLCT transitions.[48]

The toluene solutions of the compounds exhibited very low photoluminescence quantum yields (PLQYs; Φ_{tol}) (Table 1). In

the solid state, PLQYs (Φ_{film}) were found to be in the range from 2% for K5 to 7% for K2, pointing to the occurrence of SSLE. The difference between PLQYs of the neat films and of the films of the compounds doped in Zeonex (Φ_{Zeonex}) was insignificant.

The PL spectra of the dispersions of compounds in the mixtures of THF and water with different water fractions were recorded to examine the AIEE of the compounds (Fig. 4c and Fig. S24). Two competing tendencies appeared upon increasing the fraction of water (Fig. 4d). One was the emission quenching and the redshift of the PL peak caused by the polarity of water, which is significantly higher than that of THF. The other was AIEE demonstrated by the increase in PL intensity within a certain range of water fraction. Additionally, at high volume fractions of water, the precipitates of the compounds were not evenly distributed in the cuvette, affecting the measurements of the PL spectra. It should be considered as a reason for the detection of intensity drop at high volume fractions of water (Fig. 4d). The laser diffraction analysis revealed the mean size of the K2 aggregates of 31 μm in the mixture with a water volume fraction of 99% (Fig. S25).

3.3. Sensitivity of emission to picric acid

K2 was selected for the development of the detection system to highlight the multifunctionality of the compounds that can be used in OLEDs and sensors. Portions of picric acid were continuously added to the dispersions of K2 (10^{-4} M) in the mixture of THF and water (volume fraction, 95%). The intensity of PL spectra decreased upon increasing the concentration of the quencher *Q*, that is, picric acid (Fig. S26). The quenching is due to the collisional interactions of K2 in the aggregated state with the molecules of picric acid. The position of the emission peak remained the same at different concentrations of picric acid. The PL spectra were in good agreement with the respective spectra shown in Fig. 3a. This observation indicates that picric acid is non-emissive and does not have any contribution to the spectra. The Stern–Volmer relationship describing the dependence of the change in PL intensity of the samples after adding the quencher I_0/I on the molar concentration of picric acid was studied (Fig. 4e).[42] At quencher concentrations lower than 170 μM, a downward curvature of the Stern–Volmer plot was observed (Fig. 4e, inset). It is attributed to the existence of a dual response of the aggregates of K2 to the picric acid. It is caused by the partial inaccessibility of K2 molecules to picric acid due to the size of the precipitates. The Stern–Volmer plot was built for the range of low concentrations of picric acid using the equation[49]

$$\frac{I_0}{I} = \left[\frac{f_1}{1 + K_{SV1}[Q_{PA}]} + \frac{f_2}{1 + K_{SV2}[Q_{PA}]}\right]^{-1},$$

The adjusted R^2 value of the fit was calculated to be 0.998. The Stern–Volmer plot revealed fractions f_1 of 10% and f_2 of 90%. These factors are related to the emissions that have different sensitivities to picric acid. The corresponding Stern–Volmer constants K_{SV1} and K_{SV2} were found to be 16.2×10^4 and 2.7×10^3 M^{-1}, respectively. With respect of the value of K_{SV1}, K2 (limit of detection, 144 ppb) outperforms previously reported emitters (Table S2b).[50–55] At higher molar concentrations of picric acid, the curvature of the Stern–Volmer relationship exhibited an upward trend as it was expected for the detection systems of picric acid.[51,52] The upward curvature points to a combination of static and dynamic quenching and the self-absorption of picric acid.[51,52,56,57] The absence of the spectral overlap between the absorption of picric acid[58] and the emission of K2 (Fig. 3a) effectively excludes the resonance energy transfer as a mechanism of emission quenching.[26] Consequently, the CT is a driver of the sensitivity of emission to picric acid. The formation of the complex of K2 and picric acid was examined using the DFT calculations (B3LYP/6-31G(d,p)). The proximity of picric acid to the regions of high electron density of K2 leads to electrostatic interactions responsible for emission quenching. Both dicyanoisophorone and phenylcarbazole fragments act as electron donors for picric acid. The interaction energy was estimated to be –21.38 kcal mol^{-1} (Fig. S27).

The selectivity tests were performed to evaluate the potential of the detection system for practical application (Fig. 4f). With this purpose, the sensitivities of the emission of K2 to picric acid and other contaminants (10 μg mL^{-1} in samples described in Fig. 4f) were tested. Sodium 3-nitrobenzenesulfonate (Na-3NBZS) is often detected in chemical wastes and pesticides. In addition, the effects of the presence ammonium chloride (as a typical fertilizer); ammonium acetate (commonly used as a reagent for soil testing and being a component of industrial waste); 2-bromophenol (as a byproduct of pesticide and flame-retardant production); benzene, *p*-xylene, and toluene (abundant in industry and automobile exhausts and pesticides); and 2,4,6-trinitrotoluene (TNT) (as another nitroaromatic explosive material) were estimated. The addition of bromophenol and benzene did not only fail to quench the PL of aggregates of K2 but slightly enhanced the emission. The addition of Na-3NBZS, ammonium chloride, and TNT practically did not have any impact on the emission of K2. The formation of the complexes of K2 with picric acid led to a considerably higher quenching rate compared with that observed in the presence of ammonium acetate, *p*-xylene, and toluene, demonstrating relatively strong selectivity of the K2-based detection system. It is important to underline the different mechanisms of quenching of the emission of K2. For example, although toluene and benzene are both non-polar solvents, they directly suppressed the aggregate formation of K2 due to the solvation effects, leading to the reduction of AIEE.

3.4. Performance in WOLED

K2 was selected to test its EL performance due to the highest values of hole and electron drift mobilities and one of the highest PLQYs of the film in the series. OLED of the following structure was fabricated: ITO/HAT-CN (15 nm)/TCTA (35 nm)/mCP (10 nm)/K2:mCP (20 nm, 5 wt%)/TSPO1 (5 nm)/TPBi (45 nm)/LiF (0.4 nm)/Al (ESI). The layers of mCP and guest–host system were consecutively deposited. This resulted in the appearance of two peaks in the EL spectrum at ~375 and

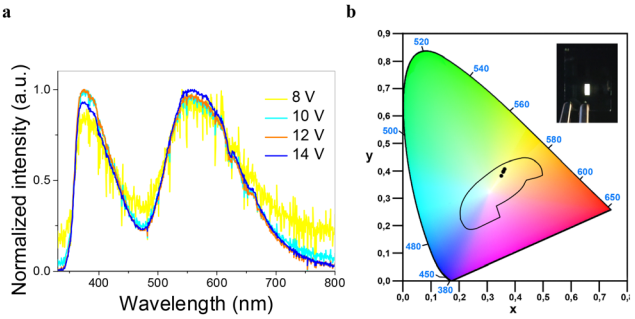

Fig. 5 K2-based OLED: (a) EL spectra. (b) The 1931 CIE color space diagram with the area designated for white-color emission.[22] Inset: Photograph of the device.

555 nm (Fig. 5a). The recombination zone occurred at the interface of the layers. The peak at ~375 nm is the signature EL band of mCP.[59] The peak at 555 nm corresponds to the PL spectrum of K2, pointing to the efficient electronic excitation energy transfer from mCP to K2. The combination of the violet and yellowish green emissions resulted in the formation of white light (Fig. 5b) with the Commission Internationale de l'Eclairage (CIE) coordinates of the standards of different years presented in Table S2a.[60] The EL spectra of the WOLED underwent slight changes with increasing voltage (Fig. 5a). The WOLED at 8 V exhibited a CRI of 82 and a correlated color temperature (CCT) of 4910 K, which is attributed to the neutral CCT near the edge of cool white light (Table S2a).[61] The device showed an external quantum efficiency (EQE) of 1.4%, comparable with the performance of other WOLEDs with a single emitting layer based on AIEEgens (Table S2b, Fig. S33). Considering the moderate PLQY of the film of K2 in air, the EQE of 1.4% is partially attributed to the utilization of HLCT states with no emission quenching by oxygen.

3.5. Quadratic hyperpolarizability

To rationalize the NLO response of the chromophores, second-order NLO polarizability (first/quadratic hyperpolarizability, β) was estimated using the hyper-Rayleigh scattering (HRS) technique (SI Section S1) in toluene and DMF.

The results, as summarized in Table 2, were interpreted within the framework of the undamped two-level model (SI Section S8 and eqn (S1)).[45] The resonance-corrected first hyperpolarizabilities ($\beta_{HRS,0}$) follow the order K1 > K6 > K2 > K5, consistent with the donor strength of 9-phenyl-9*H*-carbazole > 9,9-dimethyl-9*H*-fluorene > 9*H*-fluorene > phenanthrene for toluene solutions. Compound K1, bearing the strongest donor, exhibits the highest $\beta_{HRS,0}$ (66×10^{-30} esu) (Table 2) for toluene, correlating with its lowest excitation energy (E_{10} = 2.50 eV), largest dipole change ($\Delta\mu$ = 30.43 D), and greatest donor charge redistribution (Δq_D = 0.39406) (Table S3). Despite higher molar absorptivity (44 054 M^{-1} cm^{-1}) and oscillator strength (0.6224), K5 shows the lowest $\beta_{HRS,0}$ due to its higher E_{10} (2.65 eV). K2 and K6 exhibited comparable β values within the experimental error. Solvent polarity effects were inconsistent: $\beta_{HRS,0}$ increased almost 1.2-fold for K2 and K5, but decreased by 1.7- and 1.2-fold for K1 and K6, respectively, upon switching from toluene to DMF.

The intrinsic first hyperpolarizability ($\beta_{o,int}$), as proposed by Kuzyk, provides a more reliable metric for evaluating materials for device applications.[62] Despite possessing the lowest number of polarizable electrons (N = 18), the compounds K2 and K6 exhibited size-independent $\beta_{o,int}$ values, comparable in magnitude with those of K1. By contrast, K5, which has the highest number of polarizable electrons (N = 26), displayed the lowest $\beta_{o,int}$ value, approximately 1.3-fold lower than K1 and K6 and 1.2-fold lower than K2 (Table 2 and Fig. S34a). Nevertheless, this trend is consistent with the relative donor strengths discussed earlier. Notably, $\beta_{o,int}$ decreased twofold for K1 from toluene to DMF (highlighted in blue, Fig. 6a), whereas its impact on other members remained relatively minor. Perhaps, the presence of a heteroatom in K1 probably makes its β values more sensitive to solvent polarity by modulating the equilibrium between quinoid and aromatic ground-state forms (Fig. S34b).

The tensorial nature of β is depicted by the depolarization ratio (ρ), which also underpins the molecular symmetry (ρ value

Table 2 Quadratic NLO parameters of K1–K6

	Solvent	N^a	E_{10}, eV^b	λ_{max}, nm	$\beta_{HRS}{}^c$	$\beta_{HRS,0}{}^d$	$\beta_{theo}{}^e$	$\beta_{zzz}{}^f$	$\beta_{zzz,0}{}^g$	$\beta_{zzz,max}{}^h$	$\beta_{o,int}{}^i$	ρ^j
K1	Tol	24	2.50	425	787 ± 47	66 ± 4	267.56	1901 ± 114	160 ± 10	5687	0.028	3.81 ± 0.29
	DMF		2.46	428	481 ± 22	36 ± 2		1162 ± 54	86 ± 4	6018	0.014	3.65 ± 0.12
K2	Tol	18	2.54	424	388 ± 44	34 ± 4	171.77	937 ± 105	88 ± 10	3494	0.025	3.62 ± 0.10
	DMF		2.48	425	445 ± 11	37 ± 1		1075 ± 27	90 ± 2	3799	0.024	3.75 ± 0.23
K5	Tol	26	2.65	408	325 ± 16	46 ± 2	144.97	785 ± 39	108 ± 5	5230	0.021	4.12 ± 0.16
	DMF		2.57	410	369 ± 25	52 ± 4		891 ± 61	126 ± 9	5822	0.022	4.79 ± 0.18
K6	Tol	18	2.55	424	429 ± 28	37 ± 2	174.53	1037 ± 68	91 ± 6	3447	0.027	3.72 ± 0.12
	DMF		2.47	426	355 ± 36	38 ± 4		857 ± 88	81 ± 8	3853	0.021	3.86 ± 0.07

All samples measured at an excitation wavelength of 900 nm and all beta value results are in 10^{-30} esu. [a] Conjugated electrons involved in ICT (marked blue in the structures, Fig. S33). [b] Transition energy between the ground and excited states of the chromophore, calculated using the formula $1239.84187/\lambda_{edge}$ (Fig. S22). [c] β_{HRS}: second-order nonlinear polarizability (first hyperpolarizability). [d] $\beta_{HRS,0}$: β_{HRS} corrected for resonance enhancement using the undamped two-level model (SI Section S8 and eqn (S2)). [e] Theoretical second-order nonlinear polarizability calculated using Gaussian16 (CAM-B3LYP/6-31G/Toluene/CPCM model). [f] Calculated using SI Section S8 and eqn (S3). [g] $\beta_{zzz,0} = \beta_{HRS,0}/\sqrt{6/35}$. [h] $[\beta_{zzz}]^{max} = (3)^{1/4}[e\hbar/(m)^{1/2}]^3 N^{3/2}/E_{10}{}^{7/2}$, where e = electron charge; m = electron mass; $\hbar$ = Planck's constant and N = the number of polarizable conjugating electrons (marked in blue, Fig. S33a). [i] $\beta_{o,int}$ is the intrinsic off-resonant hyperpolarizability given by $\beta_{zzz,0}/[\beta_{zzz}]^{max}$. [j] Depolarization ratio (SI Section S8 and eqn (S4)).

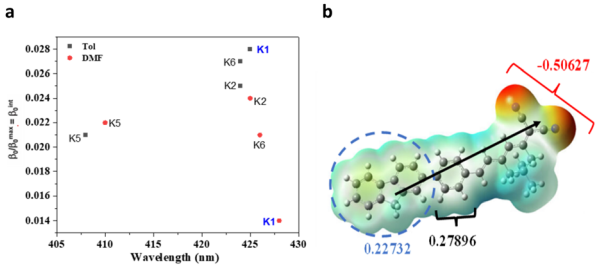

Fig. 6 Kuzyk's plot of intrinsic off-resonant hyperpolarizability (β^{int}) as a function of wavelength (λ_{max}) of molecules depicting the solvent polarity impact (a) and electrostatic potential maps of the ES of K2, calculated at the B3LYP, 6-31G(d,p) level (isosurface value of 0.002) (b). Atom color codes: C = gray; H = white; N = blue; O = red; and S = yellow (ED: electron density). The dipole direction is also presented.

is maximum up to 5 if only a single component (that is, *zzz*) is present, typically for push–pull chromophores or for purely one-dimensional dipolar chromophore).[63] With ρ values ranging from 3.62 to 4.79, these molecules can be essentially regarded as one-dimensional dipolar chromophores with a dominant hyperpolarizability tensor component (β_{zzz}). The general increase in ρ from toluene to DMF indicates enhanced CT in the polar solvent. These results agree with the theoretical analysis. The pronounced values of β and ρ confirm the non-centrosymmetric nature of the molecules, also depicted by ESP maps (Fig. 6 and Fig. S31), emphasizing their suitability as efficient NLOphores. These findings align with the theoretical analysis (Table 2 and Fig. S3, S4, Fig. 3). These β and ρ values confirm the non-centrosymmetric nature of the molecules, highlighting their potential as efficient NLO chromophores.

4. Conclusions

Derivatives of dicyanoisophorone and phenylcarbazole, fluorene, phenanthrene, or dimethylfluorene were synthesized using the Suzuki cross-coupling reaction. The synthesized compounds are characterized by high thermal stability, with 5% weight-loss temperatures of 374–378 °C. Carbazole- and phenanthrene-containing derivatives of dicyanoisophorone form molecular glasses. The compounds exhibit AIEE. The increase in photoluminescence intensity after the deoxygenation of toluene solutions of the compounds is attributed to the HLCT states. The compound containing a fluorene moiety exhibits hole and electron drift mobilities of 3×10^{-5} and 5.3×10^{-5} cm^2 V^{-1} s^{-1}, respectively, at an electric field of 5.85×10^5 V/cm. The film of the compound shows a PLQY of 7%. The ability to exhibit pronounced AIEE is confirmed by the analysis of emissions of the dispersions of the compound in mixtures of THF and water. Computational simulations and Lippert–Mataga plots demonstrate the HLCT character of the excited state of the compound and the CT mechanism of the interaction of the compound with picric acid. High sensitivity of the emission of the compound to picric acid is demonstrated with Stern–Volmer constants of 16.2×10^4 and 2.7×10^3 M^{-1} and moderately high selectivity with respect to the contaminants usually present in the environment and contaminated areas. WOLEDs fabricated using dicyanoisophorone with a fluorene moiety show a CRI of 82, CCT of 4910 K, and EQE of 1.4%. The quadratic/first hyperpolarizability value of toluene solution of the molecule containing 9-phenyl-9*H*-carbazole (K1) displayed the highest β_{zzz} of 1901×10^{-30} esu owing to its donor strength and the most asymmetric electron density distribution. This observed large nonlinear optical response may plausibly be the outcome of participation from the HLCT states. The results of this study may inspire the design and synthesis of new multifunctional dicyanoisophorone derivatives exhibiting AIEE for WOLEDs, systems for detecting nitroaromatic explosive materials, and as materials with high nonlinearities.

Author contributions

Khushdeep Kaur: investigation, writing – original draft. Oleksandr Bezvikonnyi: investigation, writing – original draft. Dmytro Volyniuk: conceptualization, investigation, methodology. Weizhen Liu: investigation, writing – original draft. Yovan de Coene: investigation, writing – original draft, funding acquisition, project administration, supervision. Koen Clays: investigation, writing – original draft. Kamaljit Singh: writing – review & editing. Ehsan Ullah Rashid: investigation. Asta Dabuliene: conceptualization, investigation. Oleksandr Navozenko: conceptualization, funding acquisition, investigation, project administration. Juozas V. Grazulevicius: conceptualization, funding acquisition, project administration, supervision, writing – review & editing.

Conflicts of interest

There are no conflicts to declare.

Data availability

The data supporting this article have been included as part of the supplementary information (SI). Supplementary information: instrumentation, synthetic procedures, thermal properties, charge-transporting properties, photophysical data, theoretical data, electroluminescence data and comparison with other compounds, NLO characteristics. See DOI: https://doi.org/10.1039/d5tc04271b.

Acknowledgements

This project has received funding from the Research Council of Lithuania (LMTLT), agreements No. S-LU-24-6 and S-A-UEI-23-1 (22-12-2023). YdC acknowledges the Fund of Scientific Research Flanders (FWO) for a senior postdoctoral fellowship (1268825N). This work has also received funding from the Ministry of Education and Science of Ukraine, agreement No M58-2024. Dr Audrius Bučinskas is acknowledged for the assistance with the laser diffraction analysis.

Notes and references

1 E. S. Moraes, J. C. Germino and L. Pereira, *Org. Electron.*, 2025, **137**, 107175, DOI: 10.1016/j.orgel.2024.107175.
2 D. Pereira, A. Pinto, A. Califórnia, J. Gomes and L. Pereira, *Mater. Sci. Eng. B*, 2016, **211**, 156–165, DOI: 10.1016/j.mseb.2016.07.004.
3 L. Popp, R. Scholz, P. Kleine, R. Lygaitis, S. Lenk and S. Reineke, *Org. Electron.*, 2019, **75**, 105365, DOI: 10.1016/j.orgel.2019.07.023.
4 T. H. Wang, L. B. Yi, S. Y. Chu and P. C. Kao, *Synth. Met.*, 2024, **301**, 117530, DOI: 10.1016/j.synthmet.2023.117530.
5 B.-Y. Lan, C.-Y. Chuang, C.-T. Tseng, J.-Y. Ke, S.-Y. Chu and P.-C. Kao, *Opt. Mater.*, 2025, **160**, 116745, DOI: 10.1016/j.optmat.2025.116745.
6 J. M. dos Santos, D. Hall, B. Basumatary, M. Bryden, D. Chen, P. Choudhary, T. Comerford, E. Crovini, A. Danos, J. De, S. Diesing, M. Fatahi, M. Griffin, A. K. Gupta, H. Hafeez, L. Hämmerling, E. Hanover, J. Haug, T. Heil, D. Karthik, S. Kumar, O. Lee, H. Li, C. F. R. Mackenzie, A. Mariko, T. Matulaitis, F. Millward, Y. Olivier, Q. Qi, I. D. W. Samuel, N. Sharma, C. Si, L. Spierling, P. Sudhakar, D. Sun, E. Tankelevičiūtė, M. D. Tonet, J. Wang, T. Wang, S. Wu, Y. Xu, L. Zhang and E. Zysman-Colman, *Chem. Rev.*, 2024, **124**, 13736–14110, DOI: 10.1021/acs.chemrev.3c00755.
7 J. C. Germino, L. G. T. A. Duarte, R. A. Mendes, M. M. Faleiros, A. de Morais, J. N. de Freitas, L. Pereira and T. D. Z. Atvars, *Nanomaterials*, 2022, **12**, 2497, DOI: 10.3390/nano12142497.
8 J. Shi, L. E. Aguilar Suarez, S. J. Yoon, S. Varghese, C. Serpa, S. Y. Park, L. Lüer, D. Roca-Sanjuán, B. Milián-Medina and J. Gierschner, *J. Phys. Chem. C*, 2017, **121**, 23166–23183, DOI: 10.1021/acs.jpcc.7b08060.
9 S. Rana, S. R. Nayak, S. Patel and S. Vaidyanathan, *J. Mater. Chem. C*, 2024, **12**, 765–818, DOI: 10.1039/d3tc03449f.
10 J. Hwang, P. Nagaraju, M. J. Cho and D. H. Choi, *Aggregate*, 2023, **4**, e199, DOI: 10.1002/agt2.199.
11 A. Afrin and P. Chinna Ayya Swamy, *J. Mater. Chem. C*, 2024, **12**, 1923–1944, DOI: 10.1039/d3tc04121b.
12 K. Clays, R. J. Docherty, J. Fielden, M. Helliwell, J. Raftery, R. Shaw, C. A. Swanson and B. J. Coe, *Nanophotonics and Macrophotonics for Space Environments IV*, 2010, vol. 7817.
13 H. Xu, D. L. Elder, L. E. Johnson, W. Heni, Y. De Coene, E. De Leo, M. Destraz, N. Meier, W. Vander Ghinst, S. R. Hammond, K. Clays, J. Leuthold, L. R. Dalton and B. H. Robinson, *Mater. Horizons*, 2022, **9**, 261–270, DOI: 10.1039/d1mh01206a.
14 P. A. Franken, A. E. Hill, C. W. Peters and G. Weinreich, *Phys. Rev. Lett.*, 1961, **7**, 118–120, DOI: 10.1103/PhysRevLett.7.118.
15 J. J. Novoa, D. Braga and L. Addadi, From Bonds to Packing: An Energy-Based Crystal Packing Analysis for Molecular Crystals Packing Analysis for Molecular Crystals, in *Engineering of Crystalline Materials Properties*, ed. J. J. Novoa, D. Braga and L. Addadi, NATO Science for Peace and Security Series B: Physics and Biophysics, Springer, Dordrecht, 2008, pp. 307–332, DOI: 10.1007/978-1-4020-6823-2_15.
16 N. Shivani, A. Mishra, P. Kaur and K. Singh, *J. Phys. Chem. C*, 2023, **127**, 1260–1272, DOI: 10.1021/acs.jpcc.2c07825.
17 L. Dai, Q. Zhang, Q. Ma and W. Lin, *Coord. Chem. Rev.*, 2023, **489**, 215193, DOI: 10.1016/j.ccr.2023.215193.
18 D. Shen, W. Jin, Y. Bai, Y. Huang, H. Lyu, L. Zeng, M. Wang, Y. Tang, W. Wan, X. Dong, Z. Gao, H. L. Piao, X. Liu and Y. Liu, *Angew. Chem., Int. Ed.*, 2021, **60**, 16067–16076, DOI: 10.1002/anie.202103674.
19 Z. Zheng, Z. Yu, M. Yang, F. Jin, Q. Zhang, H. Zhou, J. Wu and Y. Tian, *J. Org. Chem.*, 2013, **78**, 3222–3234, DOI: 10.1021/jo400116j.
20 P. Kaur and K. Singh, *Chem. Rec.*, 2022, **22**, e202200024, DOI: 10.1002/tcr.202200024.
21 M. H. Chua, K. L. O. Chin, S. J. Ang, X. Y. D. Soo, Z. M. Png, Q. Zhu and J. Xu, *ChemPhotoChem*, 2022, **6**, e202200168, DOI: 10.1002/cptc.202200168.
22 D. K. Mai, J. Lee, I. Min, T. P. Vales, K. H. Choi, B. J. Park, S. Cho and H. J. Kim, *Nanomaterials*, 2018, **8**, 728, DOI: 10.3390/nano8090728.
23 G. S. Nair, R. K. Lekshmy, K. Szaciłowski, M. Takeuchi and B. Balan, *J. Lumin.*, 2024, **276**, 120857, DOI: 10.1016/j.jlumin.2024.120857.
24 S. Maredi, S. R. Nayak, M. I. Alam, D. Thakur and S. Vaidyanathan, *J. Mater. Chem. C*, 2025, **13**, 14333–14348, DOI: 10.1039/D5TC00780A.
25 B. P. Debata, J. Dash, S. Patel and S. Vaidyanathan, *J. Mater. Chem. C*, 2025, **13**, 14385–14403, DOI: 10.1039/D5TC01672J.
26 S. M. Kumar and S. K. Iyer, *Sens. Actuators Rep.*, 2023, **6**, 100177, DOI: 10.1016/j.snr.2023.100177.
27 M. Arshad, P. Sowmya, A. Paul and A. Joseph, *Spectrochim. Acta, Part A*, 2024, **305**, 123465, DOI: 10.1016/j.saa.2023.123465.
28 S. Das, M. Das, U. K. Das, B. Chandra Samanta, A. Bag, A. Patra, N. Bhattacharya and T. Maity, *Dyes Pigm.*, 2024, **222**, 111884, DOI: 10.1016/j.dyepig.2023.111884.
29 A. D. Dwivedi, B. K. Dwivedi, M. Tripathi and D. S. Pandey, *J. Lumin.*, 2024, **273**, 120665, DOI: 10.1016/j.jlumin.2024.120665.
30 J. H. Lee, C. H. Chen, P. H. Lee, H. Y. Lin, M. K. Leung, T. L. Chiu and C. F. Lin, *J. Mater. Chem. C*, 2019, **7**, 5874–5888, DOI: 10.1039/c9tc00204a.
31 A. Srivastava, A. Srivastava, N. A. Srivastava and B. Kumar, *Opt. Mater.*, 2024, **150**, 115109, DOI: 10.1016/j.optmat.2024.115109.
32 S. Sasaki, K. Goushi, M. Mamada, S. Miyazaki, K. Miyata, K. Onda and C. Adachi, *Adv. Opt. Mater.*, 2024, **12**, 2301924, DOI: 10.1002/adom.202301924.
33 M. Ingham, A. Aziz, D. Di Tommaso and R. Crespo-Otero, *Mater. Adv.*, 2023, **4**, 5388–5419, DOI: 10.1039/d3ma00518f.
34 M. Shellaiah, W. L. Lin, P. Raghunath, K. W. Sun and M. C. Lin, *Spectrochim. Acta, Part A*, 2023, **303**, 123186, DOI: 10.1016/j.saa.2023.123186.
35 B. J. Park, K. J. Kim and T. Kim, *ACS Appl. Electron. Mater.*, 2024, **6**, 5190–5200, DOI: 10.1021/acsaelm.4c00695.
36 D. Chen, L. Zhang, T. Matulaitis, D. B. Cordes, A. M. Z. Slawin, X. H. Zhang, I. D. W. Samuel and E. Zysman-Colman, *J. Mater. Chem. C*, 2023, **11**, 13095–13105, DOI: 10.1039/d3tc02463f.
37 M. I. Alam, M. R. Nagar, D. Barman, P. K. Iyer, J. H. Jou and S. Vaidyanathan, *J. Mater. Chem. C*, 2024, **12**, 13585–13595, DOI: 10.1039/D4TC00417E.

38 A. R. Lee and W. S. Han, *Acta Crystallogr., Sect. C:Struct. Chem.*, 2015, **C71**, 195–198, DOI: 10.1107/S2053229615002624.
39 S. G. Patnaik, R. K. Gagan, R. Vedarajan, A. Yamaguchi, M. Miyauchi and N. Matsumi, *J. Electrochem. Soc.*, 2018, **165**, J3166, DOI: 10.1149/2.0231815jes.
40 S. Bejaoui and F. Salama, *AIP Adv.*, 2019, **9**, 085021, DOI: 10.1063/1.5100152.
41 V. G. Pivovarenko and A. S. Klymchenko, *Chem. Rec.*, 2024, **24**, e202300321, DOI: 10.1002/tcr.202300321.
42 U. Tsiko, O. Bezvikonnyi, D. Volyniuk, B. F. Minaev, J. Keruckas, M. Cekaviciute, E. Jatautiene, V. Andruleviciene, A. Dabuliene and J. V. Grazulevicius, *Dyes Pigm.*, 2022, **197**, 109952, DOI: 10.1016/j.dyepig.2021.109952.
43 D. K. Andrea Phan Huu, S. Saseendran, R. Dhali, L. Gomes Franca, K. Stavrou, A. Monkman and A. Painelli, *J. Am. Chem. Soc.*, 2022, **144**, 15211–15222, DOI: 10.1021/jacs.2c05537.
44 E. Lippert, *Zeitschrift fur Naturforsch. - Sect. A J. Phys. Sci.*, 1955, **10**, 541–545, DOI: 10.1515/zna-1955-0707.
45 N. Mataga, Y. Kaifu and M. Koizumi, *Bull. Chem. Soc. Jpn.*, 1956, **29**, 465–470, DOI: 10.1246/bcsj.29.465.
46 Y. S. Lee, H. Nam, Y. N. Song, W. P. Hong, W. S. Han and T. Kim, *Chem. Eng. J.*, 2025, **521**, 166658, DOI: 10.1016/j.cej.2025.166658.
47 P. Keerthika, A. Kumar, A. Selvaganesan, J. Moon, V. Nutalapati, J. Y. Lee and R. K. Konidena, *J. Mater. Chem. C*, 2025, **13**, 20540–20548, DOI: 10.1039/d5tc02737c.
48 T. H. Ha, J. Y. Yoo and C. W. Lee, *Chem. Eng. J.*, 2025, **503**, 158323, DOI: 10.1016/j.cej.2024.158323.
49 M. N. Berberan-Santos, *RSC Nanosci. Nanotechnol.*, 2016, **38**, 493–507, DOI: 10.1039/9781782622031-00493.
50 A. Ghosh, S. K. Seth, A. Ghosh, P. Pattanayak, A. Mallick and P. Purkayastha, *Chem. – Asian J.*, 2021, **16**, 1157–1164, DOI: 10.1002/asia.202100117.
51 K. Maiti, A. K. Mahapatra, A. Gangopadhyay, R. Maji, S. Mondal, S. S. Ali, S. Das, R. Sarkar, P. Datta and D. Mandal, *ACS Omega*, 2017, **2**, 1583–1593, DOI: 10.1021/acsomega.6b00288.
52 D. C. Santra, M. K. Bera, P. K. Sukul and S. Malik, *Chem. – Eur. J.*, 2016, **22**, 2012–2019, DOI: 10.1002/chem.201504126.
53 S. R. Nayak, I. Siddiqui, Shahnawaz, J. H. Jou and S. Vaidyanathan, *ACS Appl. Opt. Mater.*, 2023, **1**, 94–106, DOI: 10.1021/acsaom.2c00012.
54 S. R. Nayak, N. Shahnawaz, I. Siddiqui, J. H. Jou, S. Patel and S. Vaidyanathan, *J. Phys. Chem. C*, 2023, **127**, 499–515, DOI: 10.1021/acs.jpcc.2c05220.
55 X. D. Wang and O. S. Wolfbeis, *Chem. Soc. Rev.*, 2014, **43**, 3666–3761, DOI: 10.1039/c4cs00039k.
56 M. H. Gehlen, *J. Photochem. Photobiol., C*, 2020, **42**, 100338, DOI: 10.1016/j.jphotochemrev.2019.100338.
57 A. Weller, *Discuss. Faraday Soc.*, 1959, **27**, 28–33, DOI: 10.1039/DF9592700028.
58 P. Jana, S. Maity, S. K. Maity, P. K. Ghorai and D. Haldar, *Soft Matter*, 2012, **8**, 5621–5628, DOI: 10.1039/c2sm25062d.
59 A. Shahalizad, A. D'Aléo, C. Andraud, M. H. Sazzad, D. H. Kim, Y. Tsuchiya, J. C. Ribierre, J. M. Nunzi and C. Adachi, *Org. Electron.*, 2017, **44**, 50–58, DOI: 10.1016/j.orgel.2017.01.044.
60 N. Jarucha, Y. Ruangtaweep, P. Nawarat, P. Kanthang, P. Limsuwan, H. J. Kim, J. Kaewkhao and T. Sareein, *Integr. Ferroelectr.*, 2023, **239**, 149–157, DOI: 10.1080/10584587.2023.2234618.
61 E. K. Hansen, M. Pajuste and E. Xylakis, *LEUKOS - J. Illum. Eng. Soc. North Am.*, 2022, **18**, 30–51, DOI: 10.1080/15502724.2020.1808014.
62 P. M. Javier, Y. Zhao, K. Clays, M. G. Kuzyk, Y. Shen, L. Qiu, J. Hao and K. Guo, *J. Am. Chem. Soc.*, 2009, **131**, 5084–5093, DOI: 10.1021/ja807394f.
63 M. P. Cifuentes, C. E. Powell, J. P. Morrall, A. M. McDonagh, N. T. Lucas, M. G. Humphrey, M. Samoc, S. Houbrechts, I. Asselberghs, K. Clays, A. Persoons and T. Isoshima, *J. Am. Chem. Soc.*, 2006, **128**, 10819–10832, DOI: 10.1021/ja062246v.